ELSEVIER

Journal of Structural Geology 27 (2005) 327–342

JOURNAL OF STRUCTURAL GEOLOGY

www.elsevier.com/locate/jsg

Growth of a normal fault by the accumulation of slip over millions of years

Andrew Nicol[a,b,*], John Walsh[b], Kelvin Berryman[a], Scott Nodder[c]

[a]*Institute of Geological and Nuclear Sciences, Lower Hutt, New Zealand*
[b]*Fault Analysis Group, Department of Geology, University College Dublin, Belfield, Dublin 4, Ireland*
[c]*National Institute of Water and Atmospheric Research, P.O. Box 14901, Kilbirnie, Wellington, New Zealand*

Received 25 August 2003; received in revised form 15 July 2004; accepted 17 September 2004
Available online 24 November 2004

Abstract

Fault growth in the upper crust is mainly achieved by the accumulation of slip during earthquakes. Large faults with cumulative displacements of kilometres experience hundreds of large magnitude earthquakes but the precise manner in which maximum earthquake size evolves over millions of years is uncertain. To bridge the gap between faulting on earthquake (e.g. <100 ka) and geological (e.g. >1 Ma) timescales we examine the Cape Egmont Fault in offshore New Zealand, using good quality seismic-reflection data tied to wells and seabed bathymetry. Displacements on nine horizons, including the seabed, three horizons of 14–225 ka in age and five horizons of 5.3–1.6 Ma in age, were mapped along the ca. 70 km length of the fault. These horizons record maximum displacements ranging from 6 to 2344 m and suggest that this active fault commenced its latest phase of movement about 3.7 Ma ago. Displacement profiles for all horizons and inter-horizon increments are of similar geometry, indicating an approximately constant fault length and fixed maximum displacement position during growth. Fault length was established rapidly and inherited from an underlying Cretaceous structure with fault dimensions in the overlying sequence mainly achieved by up-dip propagation. As the magnitude of earthquakes is proportional to their rupture length, the maximum size of earthquakes on the fault remained constant for at least the last 3.2 Ma, with the distribution of slip along the fault during these events approximately comparable. This contrasts with the maximum displacement rates which varied by an order of magnitude during the last 3.7 Ma (0.18–2.8 mm/yr). Decreases in displacement rates were accompanied by proportional increases in the average earthquake recurrence intervals (ca. 1.3–18 ka), and reflect regional changes in the rates of extension.

Keywords: Fault growth; Earthquakes; Fault reactivation

1. Introduction

Large faults with cumulative displacements of a kilometre or more mainly grow in the upper crust by the accumulation of slip during large magnitude earthquakes (e.g. Gilbert, 1884; Stein et al., 1988; Walsh and Watterson, 1988; Cowie and Scholz, 1992a). As coseismic slip is small (e.g. <10 m) large cumulative fault displacements (e.g. >1 km) typically accrue during hundreds or thousands of earthquakes. Historical and paleoearthquake studies reveal much about earthquake processes over periods up to tens of thousands of years (e.g. Schwartz and Coppersmith, 1984; Lindvall et al., 1989; Sieh et al., 1989; Berryman and Beanland, 1991; Yeats et al., 1997), but few data constrain earthquake behaviour over the active life of a fault, which is often millions of years. The manner in which displacement accrues on active faults during earthquakes can vary significantly, a variability that is encapsulated in Fig. 1.

Studies of historical earthquakes and of inactive faults show that both earthquake slip and finite displacement increase with fault length (e.g. Elliott, 1976; Scholz, 1982; Bonilla et al., 1984; Watterson, 1986; Walsh and Watterson, 1988; Marrett and Almendinger, 1991; Cowie and Scholz, 1992b; Gillespie et al., 1992; Dawers et al., 1993; Wells and Coppersmith, 1994; Schlische et al., 1996). For inactive fault systems these relationships are most often interpreted to directly reflect fault growth, with repeated earthquakes on a fault producing an increase in both cumulative displacement and fault length (Fig. 1c–f). Increases in fault dimensions are achieved by tip-line propagation (e.g.

* Corresponding author. Tel.: +64-4-5701444; fax: +64-4-5704600
E-mail address: a.nicol@gns.cri.nz (A. Nicol).

0191-8141/$ - see front matter © 2004 Elsevier Ltd. All rights reserved.
doi:10.1016/j.jsg.2004.09.002

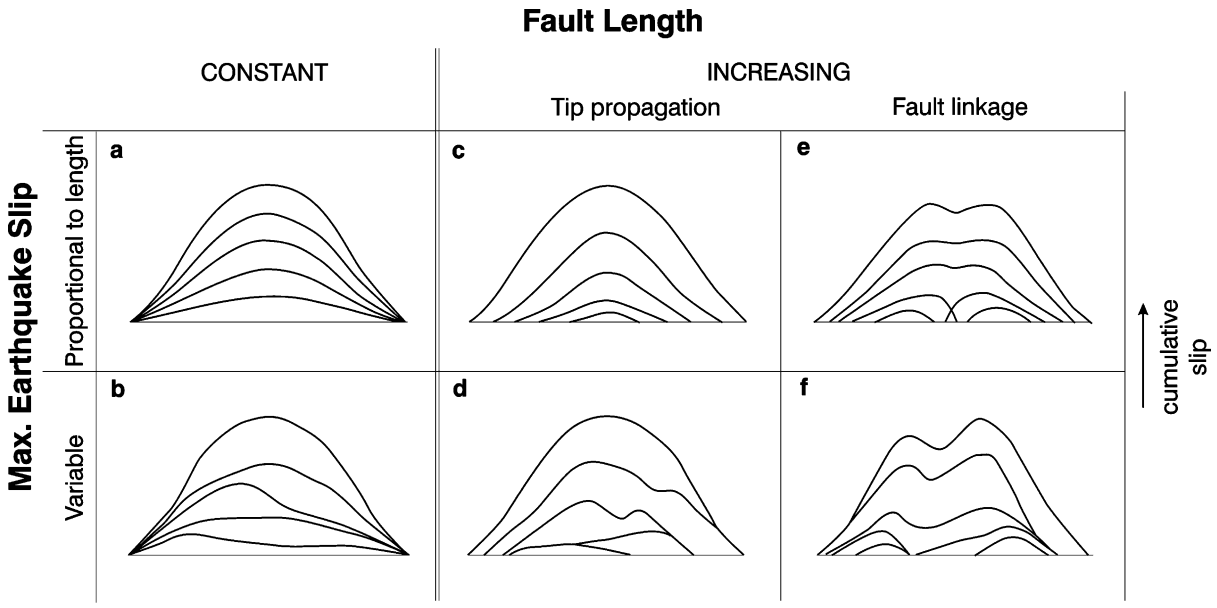

Fig. 1. Schematic diagrams showing models for the accumulation of fault slip during repeated earthquakes. The six models show variants of the constant length and increasing length fault growth models together with the characteristic and variable earthquake-slip models (see Schwartz and Coppersmith, 1984; Walsh and Watterson, 1988; Scholz, 1990; Walsh et al., 2002). These models apply to faults with cumulative displacements that decrease from a centrally located maximum and are end-members in a continuum. All of the models may include soft-linked fault segments (i.e. fault segments that form part of a single kinematically coherent array).

Walsh and Watterson, 1988; Cowie and Scholz, 1992a; Gillespie et al., 1992), which may, in some instances, be accompanied by linkage of initially isolated faults (e.g. Trudgill and Cartwright, 1994; Cartwright et al., 1995; McLeod et al., 2000). This fault growth model does not, however, adequately account for the formation of some fault arrays in which trace lengths were established rapidly (within the first 10–20% of the period of faulting), and growth for much of the duration of faulting was achieved by increases of displacement with near constant fault lengths (Morewood and Roberts, 1999; Meyer et al., 2002). This type of growth is, however, consistent with an alternative fault growth model (Walsh et al., 2002), hereafter referred to as the constant fault-length model, in which growth is accomplished by increasing cumulative displacement and near constant fault lengths. The constant fault-length model reconciles fault displacement and length-scaling relationships on earthquake and geological time scales and is consistent with self-similar coseismic-slip distributions which suggest no discernible increase in fault length at short time scales (e.g. Lindvall et al., 1989; Grant and Sieh, 1994).

The constant and increasing fault-length models are illustrated in Fig. 1, where increases in fault length could be achieved by tip-line propagation of a single fault (Fig. 1c and d) and/or by linkage of multiple faults (Fig. 1e and f). It is important to recognise that faults growing in association with either the constant or increasing fault-length models may, in detail, comprise an array of soft-linked and kinematically coherent segments (Walsh and Watterson, 1987, 1991; Walsh et al., 2003). Such kinematically related segments may be hard linked at depth and could all rupture during a single earthquake. Therefore, the above models cannot be discriminated on the basis of their small-scale fault segmentation characteristics, which arise from segmentation processes accompanying the localisation of individual faults within rock volumes (e.g. Mandl, 1987; Childs et al., 1995; Treagus and Lisle, 1997; Walsh et al., 2003).

The models in Fig. 1 apply to faults with cumulative displacements that decrease from a centrally located maximum and are end-members in a continuum. In each model, growth may be achieved by systematic accumulation of earthquake slip throughout the life of a fault (Fig. 1a, c and e) or alternatively by variable slip increments (Fig. 1b, d and f). Which, if either, of the two basic fault-growth models (i.e. constant or increasing fault-length) best describes earthquake behaviour over millions of years has not been resolved. The distinction between these models is, however, critical, as progressive increases in fault length require a progressive rise in the maximum earthquake magnitude and, for constant slip rates, a decrease in earthquake recurrence intervals. This contrasts with the constant fault-length model for which constant slip rates can arise from invariant earthquake maximum magnitude and recurrence interval.

Limitations in our current understanding of how incremental slip during individual earthquakes or earthquake cycles accumulates to produce finite displacement arise partly due to a lack of suitable data. The best fault data are

most often from inactive fault arrays, such as are preserved in the North Sea, which provide limited insight into the earthquake faulting process. This contrasts with active fault systems which can provide very useful constraints on earthquake faulting, but often yield little information on fault evolution over millions of years. For example, the Wasatch Fault in western USA has experienced, at individual sites, up to six large magnitude earthquakes over the last 6–13 ka (Machette et al., 1992; McCalpin et al., 1994); however, erosion on the upthrown side of the fault has destroyed evidence of the long-term history of displacement accumulation on the fault.

To address questions of how the accumulation of slip in large magnitude earthquakes produces long-term (i.e. hundreds of thousands to millions of years) fault growth requires special data sets with active faulting at the ground surface or seabed, preservation of syn-faulting horizons, age control for displaced surfaces spanning a significant portion of the life of a fault and good quality sub-surface data (e.g. seismic reflection profiles or wells). The geological conditions required to preserve the syn-faulting strata necessary to elucidate fault-growth histories are not widely reported in the literature and demand a delicate balance to be maintained between the rates of sedimentation, erosion, regional tectonic uplift and fault displacement. The Cape Egmont Fault (CEF) in the Taranaki Graben, offshore New Zealand, satisfies these requirements, with a seabed fault scarp and eight displaced horizons ranging in age from 14 ka to 5.3 Ma BP, which can be mapped along the length of the fault using seismic-reflection lines. Displacement of these horizons constrains incremental fault growth for periods of time during which the number of earthquakes ranged from one or two to hundreds. They allow us to assess the stability of the fault growth process and, in particular, to estimate the stability of slip magnitude and the recurrence of maximum magnitude earthquakes over timescales up to millions of years.

We discuss this topic at a first-order level and consider only those large magnitude earthquakes ($>$M6) that ruptured significant portions of the CEF (total length 70 km) and that could potentially be recorded in paleoseismic trenching studies if this structure cropped out on land. These large magnitude events may be sampled from earthquake populations that range from being Characteristic (uniform) to Gutenberg–Richter (power-law) (Wesnousky, 1994). This approach is acceptable even when earthquakes on a fault have a Gutenberg–Richter relation, because although events with large magnitudes represent a small proportion of the total earthquake population, they contribute a significant proportion ($>$80%) to the total slip on the fault (Nicol et al., 2004).

2. Geological background and data

The CEF is located in the offshore portion of the Taranaki Basin up to 100 km west of the North Island of New Zealand and within the continental crust of the Australian Plate (Fig. 2). The fault is currently accommodating normal displacement and south of Cape Egmont defines the western margin of the Taranaki Graben, a zone of backarc extension, which is driven by subduction of the Pacific Plate along the Hikurangi margin, and extends for at least 250 km in a north-northeast direction (Fig. 2). The CEF is ca. 70 km long, dips ca. 60–70° to the east and varies in strike from northeast (035°) to east-northeast (065°) with changes in fault strike often occurring along fault branch lines to synthetic splays (Figs. 3, 5 and 6). In addition to these splays a number of antithetic faults occur in the hanging wall of the main fault.

The CEF has a maximum throw on Pliocene–Pleistocene horizons of about 2300 m and is the largest normal fault in the Taranaki Graben at this latitude (Thrasher, 1990, 1991; King and Thrasher, 1992, 1996; Nodder, 1993, 1994). The remainder of normal faults in the graben have throws of 70–700 m on the base Pliocene horizon, dip both east and west, and strike approximately parallel to the graben (Fig. 2; Thrasher et al., 1995). Within the map area the largest of these faults forms an antithetic to the main fault at its northern end (Fig. 3) and transfers displacement further northwards.

The Taranaki Basin has been subjected to two phases of extension, during the Late Cretaceous (ca. 65–80 Ma) and Pliocene–Recent (ca. 0–5 Ma), which on the CEF were separated by contraction during the Late Miocene (ca. 5.5–7.5 Ma: Thrasher, 1990, 1991; King and Thrasher, 1992, 1996). These phases of deformation are indicated by thickness changes of Late Cretaceous, Late Miocene and Pliocene–Pleistocene strata across the fault which are illustrated in Fig. 2 (cross-section B–B′) and Fig. 4. We concentrate on the latest period of extension. Post-Miocene faulting in the Taranaki Graben accommodates 2–4% extension in an approximate east–west direction on faults that are resolved by seismic-reflection data (i.e. with throws down to about 30 m: Thrasher, 1991; King and Thrasher, 1996).

Historical seismicity in the Taranaki Graben indicates active deformation in the crust (Robinson et al., 1976; Reyners, 1989), while the seabed scarp along the CEF confirms that this fault is active (van der Linden, 1971; Nodder, 1993, 1994). In onshore New Zealand, the formation of fault scarps usually requires large magnitude earthquakes (Berryman and Beanland, 1991) and we infer this also to be true of the CEF; this assumption is not a prerequisite for our analysis of fault displacements and growth.

The CEF is resolved by good quality seismic-reflection and seafloor bathymetric surveys covering a region 80 km long and up to 35 km wide (Figs. 3 and 7). These seismic data are of three basic types; (i) 36 multi-channel oil industry seismic lines with a mean spacing of 2 km and recorded to 5 s two-way travel time (TWTT; e.g. see Fig. 5), (ii) shallow (upper 300 ms TWTT) single-channel seismic lines (e.g. Fig. 6) and (iii) 3.5 kHz seismic lines which image faults and folds in the upper 30 ms TWTT. The 20 single-channel and 3.5 kHz

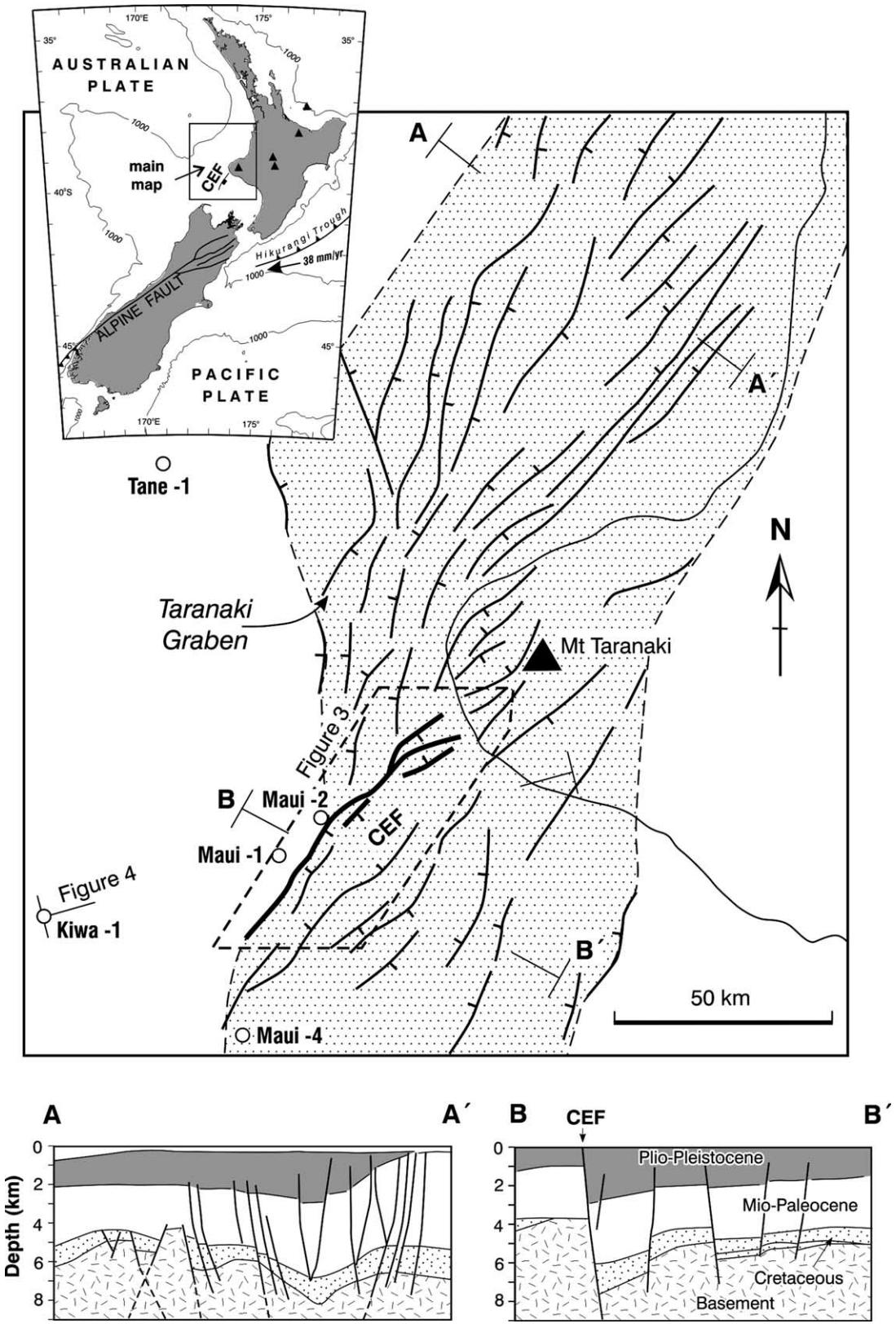

Fig. 2. Maps showing the New Zealand plate boundary (inset map) and Pliocene–Pleistocene normal faulting in the Taranaki Graben (main map). Main map modified from King and Thrasher (1996). Cross-sections A–A′ (modified from Thrasher et al. (1995)) and B–B′ (King and Thrasher, 1996; this study) across the northern and southern ends of the graben (see map for location). Location of the Cape Egmont Fault (CEF) and Figs. 3 and 4 are indicated on the main map. Inset map shows locations of active volcanoes (filled triangles), while the filled arrow shows the relative plate motion vector from DeMets et al. (1994).

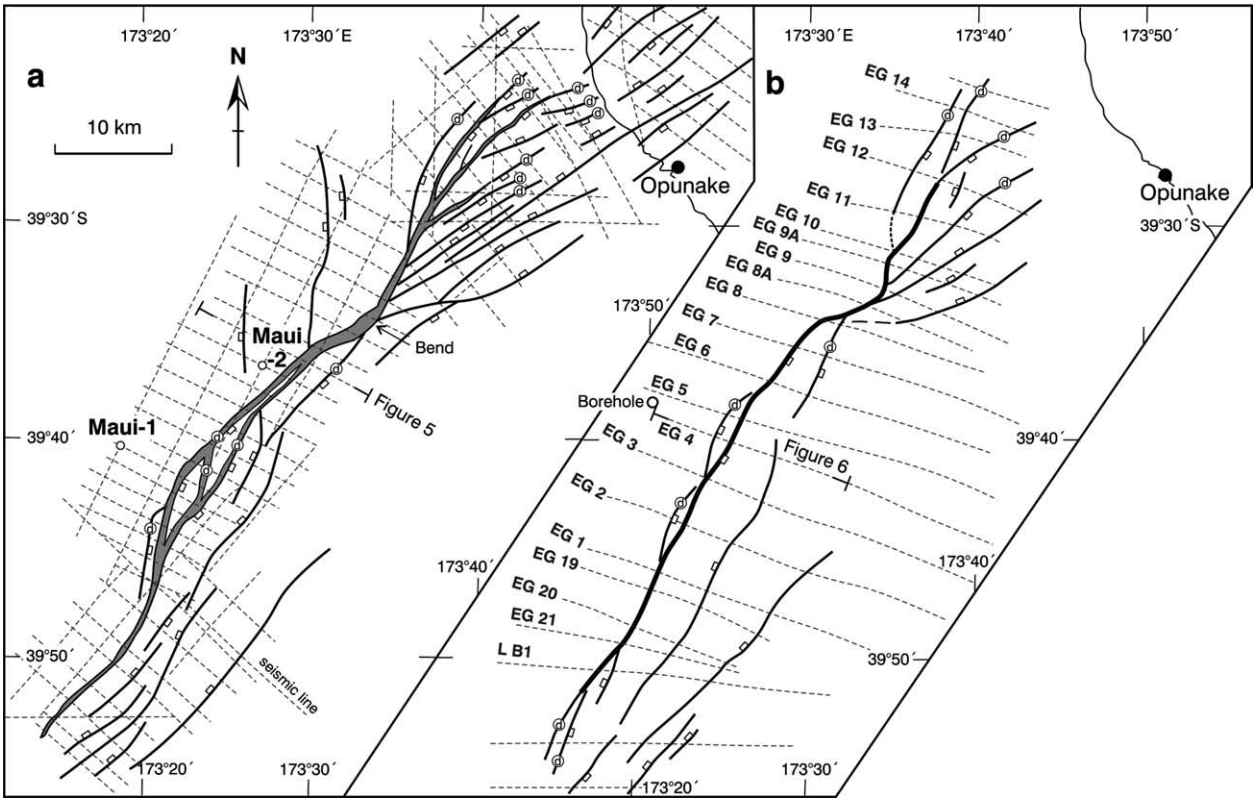

Fig. 3. Maps of the Cape Egmont Fault on the (a) 3.7 Ma and (b) Late Quaternary horizons. Thick line marking the fault trace on (b) indicates the approximate location of the seabed scarp. Locations of seismic-reflection lines used in this study are shown (thin dashed lines). Locations of Figs. 5 and 6 indicated. See Fig. 2 for location.

seismic data are principally from Nodder (1993, 1994) and have a mean line spacing of 3.5 km (Fig. 3b).

Five Plio-Pleistocene horizons were interpreted within the deep multi-channel data set (e.g. Fig. 5) and have ages of approximately 5.3 Ma (base Pliocene and Opoitian NZ stage), 3.7 Ma (base of Waipipian NZ stage), 3.2 Ma (base of Mangapanian NZ stage), 2.6 Ma (base of Nukumaruan NZ stage) and 1.6 Ma (base of the Castlecliffian NZ stage). Ages for these interpreted horizons have been determined by tying seismic reflectors to the Maui-2, Maui-4, Kiwa-1 and Tane-1 wells (Figs. 2 and 3). Biostratigraphic age determinations are from well completion reports (Shell BP Todd Services Ltd, 1970a,b, 1977, 1982) with modifications from M. Crundwell (pers. comm., 2000) and are estimated to be ±5%. Within the Late Quaternary sequence, ages for interpreted horizons were determined by correlations to the oxygen isotope record based on radiocarbon dates and nannofossil assemblages from piston cores and a 160 m deep borehole; for location see Fig. 3b and for details of stratigraphy refer to Nodder (1993, 1994). Displacement data for three Late Quaternary horizons with estimated ages of ca. 225 ka (oxygen isotope stage 7a), ca. 124 ka (oxygen isotope stage 5e) and ca. 14 ka (oxygen isotope stage 2) are utilized in this paper. Uncertainties on the ages of Late

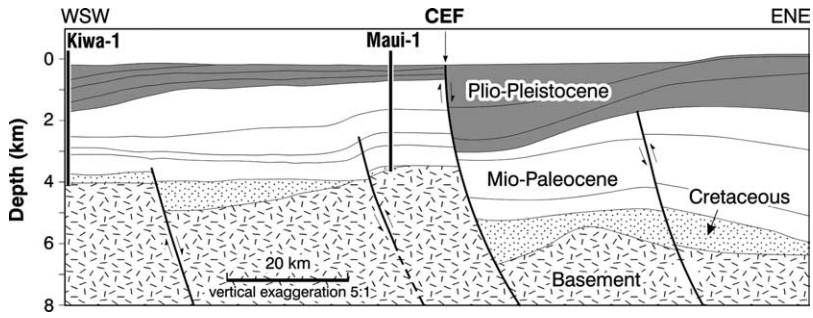

Fig. 4. Regional cross-section across the Cape Egmont Fault modified from Thrasher et al. (1995). Changes in the thickness of the Cretaceous and younger strata provides an indication of the fault displacement history. The fault experienced normal displacement in the Late Cretaceous and Pliocene–Pleistocene and reverse movement in the Late Miocene.

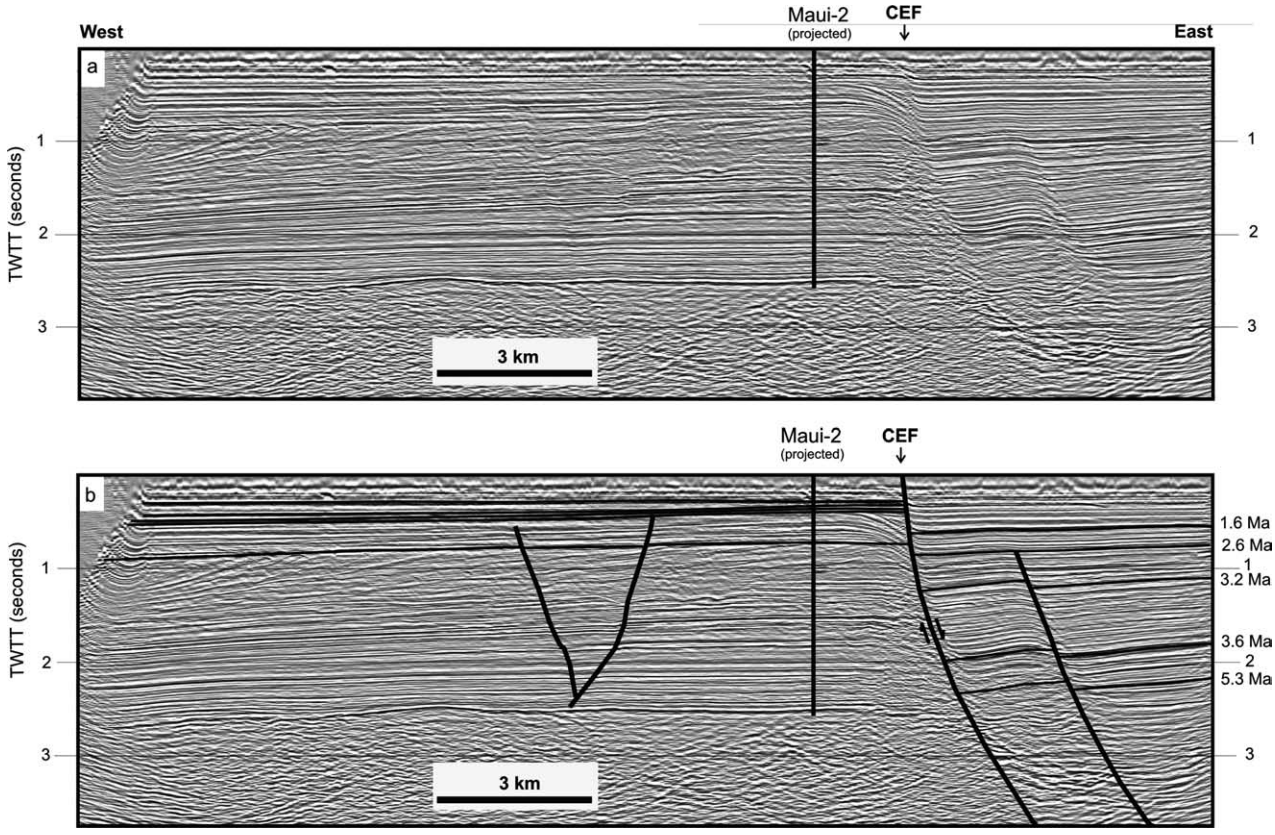

Fig. 5. Example of a deep industry seismic profile (line 86ma-46) across the Cape Egmont Fault. (a) Uninterpreted and (b) interpreted sections shown (see text for further discussion of interpretation). Location of the seismic line is shown on Fig. 3a. Vertical exaggeration is approximately ×1.5 in the upper 2 s.

Quaternary horizons could be of the order of ±10–15%. Seabed bathymetry reveals a fault scarp up to ca. 6 m in height (Fig. 7). Although the age of the seabed scarp is unknown, its presence suggests that fault displacement rates exceeded differential sedimentation rates across the fault (ca. 0.7–0.8 mm/yr) in the Late Holocene from which we infer that the fault ruptured the seabed one or more times during this time interval.

3. Comparison of short- and long-term fault growth patterns

During the post-Miocene period, average long-term sedimentation rates in the hanging wall of the CEF are greater than fault displacement rates. This condition results in the fault being blanketed by sediments, preserving its displacement history as across-fault thickness changes of syn-faulting sedimentary intervals. During the period of fault activity successively older syn-faulting horizons have progressively more displacement with the difference in displacement between two horizons principally reflecting the horizon ages and the fault-displacement rate (e.g. Petersen et al., 1992; Childs et al., 1993, 1995, 2003).

Vertical displacements on the CEF, i.e. fault throws (Figs. 8 and 9), were recorded as differences in TWTT

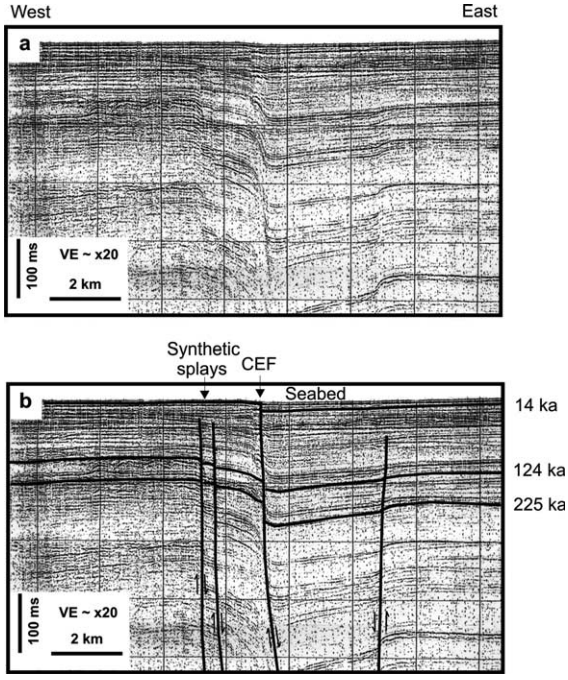

Fig. 6. Example of a single channel seismic-reflection profile for line EG 4 (modified from Nodder (1994)). (a) Uninterpreted line and (b) interpreted seismic line. Refer to Nodder (1994) for the acquisition parameters and to the text for further discussion of the interpretation. Location of the profile is shown on Fig. 3b. Vertical exaggeration is approximately ×20.

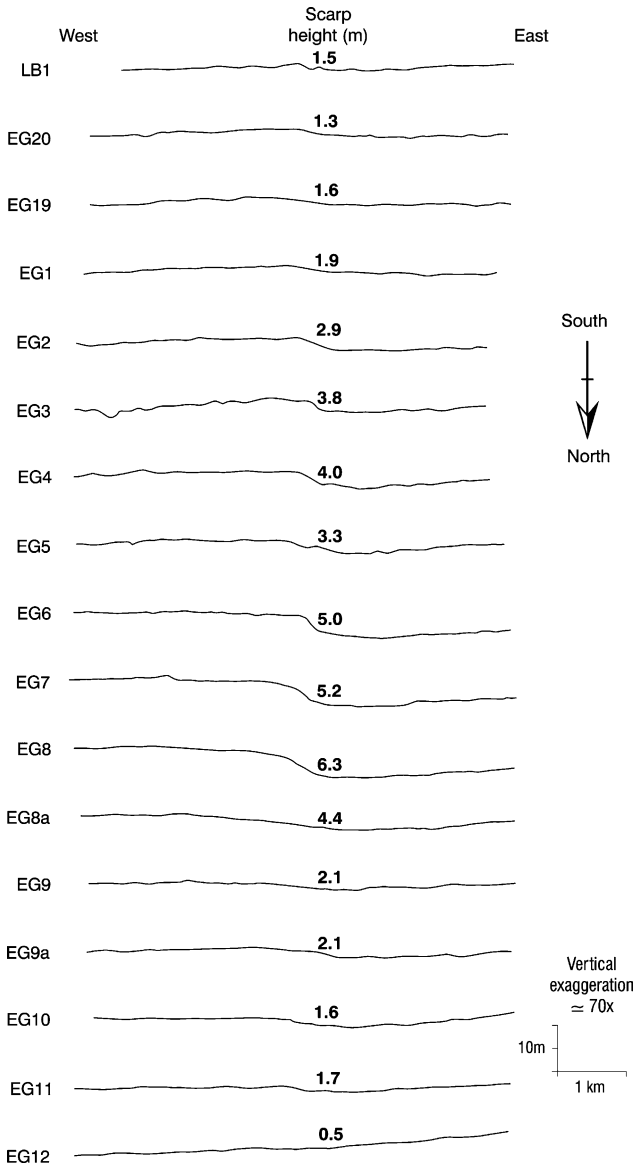

Fig. 7. Seabed scarp profiles along the length of fault (modified from Nodder (1993)). Location of the profiles is shown on Fig. 3b.

between footwall and hanging wall horizon cutoffs and have been converted to depth for the Pliocene–Early Pleistocene sequence using an average for the velocity–depth curves from the Maui-2 and Maui-4 wells (Shell BP Todd Oil Services, 1970a,b). Displacements on Late Quaternary horizons were determined using an average velocity of 1650 m/s, while the height of the seabed scarp was estimated using a velocity of 1500 m/s for water (Nodder, 1993). Adjustments in our preferred velocity–depth model could result in an error of up to ±10% in throw for the 1.6–5.3 Ma sequence. In addition, up to a further ±5% may arise due to errors in the horizon correlation and in the locations of horizon cutoffs. Lastly, the displacements do not incorporate decompaction of the growth sequence. Compaction will have the effect of decreasing displacements on all horizons by an amount that is no greater than ca. 20% (Fault Analysis Group, unpublished work). Our estimates of uncertainty for a variety of factors provide total errors that may reach a maximum of +15% and −35% for displacements of horizons in the Pliocene–Pleistocene sequence. Based on data presented in Nodder (1993, 1994) we estimate uncertainties on displacements of the Late Quaternary horizons to be of a similar order (±20–30%), while local erosion of, and sedimentation against, the seabed scarp mean that measurement of its height is typically associated with errors of about ±20–50%. As uncertainties arising from depth conversion and decompaction are likely to have a similar impact for displacements measured on the same horizon and from adjacent seismic lines, the shapes of profiles in Fig. 9 are likely to be more stable than would be suggested by the total maximum errors.

The displacement profiles in Figs. 8 and 9 display aggregate throws for the main fault and its synthetic splays (see Fig. 3 for locations of synthetic splays) plotted against horizon age and distance along the fault, respectively. For both Pliocene–Early Pleistocene horizons (Figs. 8a and 9a) and Late Quaternary horizons (Figs. 8b and 9b), displacements are aggregated because we are primarily concerned with the first-order displacement relations and not the segmentation within the fault zone. Vertical displacement profiles of present-day throw on horizons of variable age reflect incremental changes in displacement and constrain the growth of the CEF since 5.3 Ma BP (Fig. 8a and b). These profiles indicate that displacement rates varied in time. Little or no displacement accrued between approximately 5.3 and 3.7 Ma, reflected in near-constant across-fault thicknesses of strata for this time interval. Strata deposited during the period 3.7–3.2 Ma BP show substantial increases in the thickness from footwall to hanging wall, consistent with up to about 1300 m of throw accruing on the fault during this 0.5 Ma period of time. Therefore, the present period of extension commenced at about 3.7 Ma and was preceded by at least 1.5 Ma of tectonic quiescence. Following 3.2 Ma the fault accumulated up to 1000 m of displacement, with a maximum of 600 m accruing before 1.6 Ma and up to 85 m after 225 ka.

Displacement profiles in Fig. 9 utilise most of the data in Fig. 8 and show systematic variations in throw along the length of the fault for each of the dated horizons in the growth sequence (i.e. 3.7, 3.2, 2.6 and 1.6 Ma; 225, 124 and 14 ka) and for the seabed scarp. The strike-parallel profiles show a progressive reduction in maximum displacement and average displacement gradients for decreasing horizon age, with younger horizons recording less of the displacement history. The long-term displacement profiles in Fig. 9a are reminiscent of symmetrical bell-shaped or linear profiles with centrally located maxima (between ca. 33 and 45 km along the fault) separating parts of the fault with approximately equal throw gradients (see Muraoka and Kamata, 1983; Barnett et al., 1987; Walsh and Watterson, 1988; Peacock and Sanderson, 1991). Displacement profiles for Late Quaternary horizons in Fig. 9b, although more

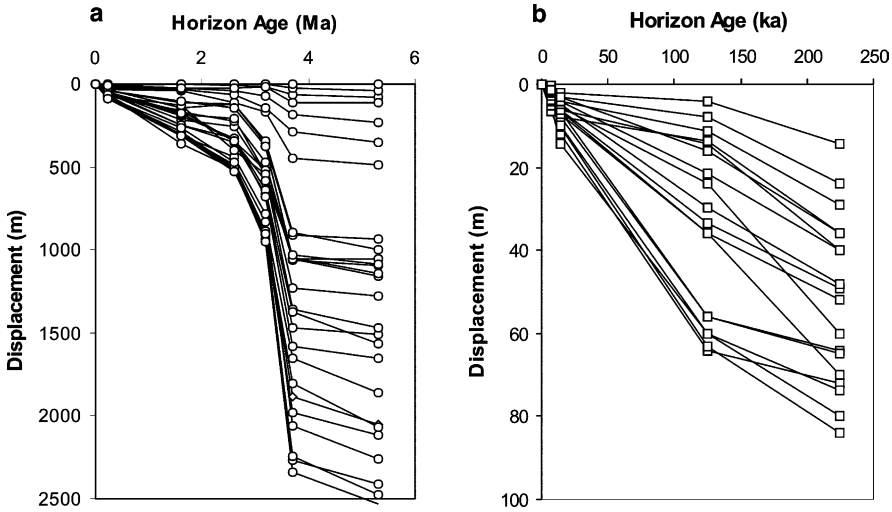

Fig. 8. (a) Vertical profiles of displacement versus horizon age for each deep seismic line crossing the Cape Egmont Fault (see Fig. 3a). (b) Vertical profiles of displacement versus horizon age for Late Quaternary horizons and the seabed scarp measured on each seismic line on Fig. 3b. For the purposes of this plot the seabed scarp has been assigned an age of 7 ka. (a) Shows the onset of deformation at about 3.7 Ma, with changes in rates of displacement through time. The variable positions of displacement profiles for each seismic line are indicative of along-strike changes in displacement (see also lateral displacement profiles in Fig. 9).

variable than those in Fig. 9a, are also characterised by displacements that increase to maxima at distances of 35–40 km along the fault. Superimposed on these broad displacement patterns, local fluctuations in displacement can be observed. The most pronounced of these changes occurs between 40 and 50 km along the fault, and coincides with a prominent bend in the trace (Fig. 3). From the bend northwards a component of displacement may have been transferred away from the fault to unresolved ductile strains and/or to antithetic faults in the hanging wall of the main slip surface. This transfer of displacement persisted throughout much of the last 3.7 Ma.

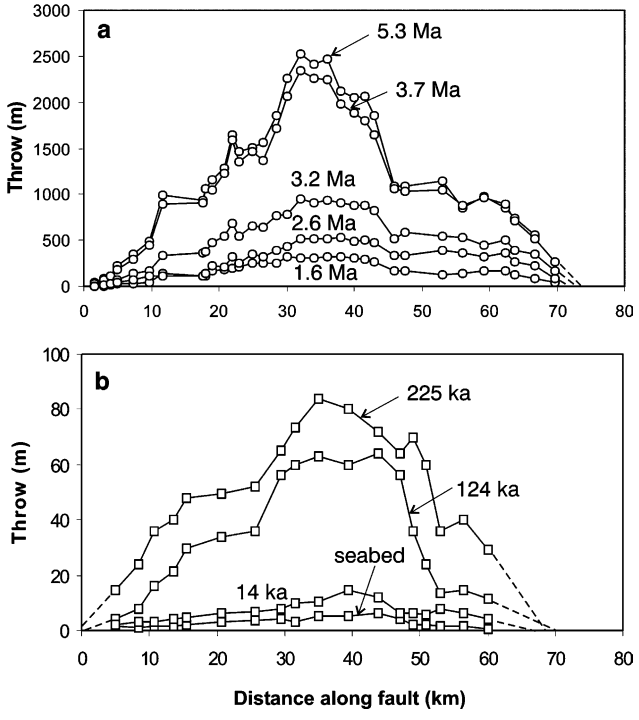

Fig. 9. Lateral (along-strike) profiles of displacement for the Cape Egmont Fault. Distance along the fault trace measured from the southern tip on the base of the growth sequence (i.e. 3.7 Ma horizon). (a) Profiles for faulted horizons dated at ca. 5.3, 3.7, 3.2, 2.6 and 1.6 Ma. (b) Profiles for faulted horizons with estimated ages of ca. 225, 124 and 14 ka and for the seabed scarp. See text for further explanation of the data.

The two sets of profiles in Fig. 9a and b are compared directly in Fig. 10a by normalising throw to the maximum displacement for each profile. The normalised profiles in Fig. 10a confirm that, to a first order, the along-strike distribution of displacement is similar for each horizon and independent of horizon age. Similarly, the incremental throw profiles in Fig. 10b (see caption for derivation), although more variable than the cumulative profiles (as would be expected given that they were derived using two profiles in Fig. 10a), also indicate a measure of stability in the geometry of the displacement profiles. These plots show that the location of the maximum displacement appears not to have changed significantly over periods of time spanning the last few earthquakes (i.e. last 10–14 ka) to the inception of the present normal fault at 3.7 Ma. This stability requires that the location of the basin centre in the hanging wall of the fault also remained approximately fixed for the duration of faulting, as has been described for the Lupa Fault in the Rukwa Rift (Morley et al., 2000). Despite the broad stability of displacements, Late Quaternary profiles are slightly more asymmetric than those of the older horizons with higher displacement gradients north of the throw maxima than to the south. This slight change in the asymmetry of the displacement profiles is attributed to the more distributed nature of the fault zone to the north and to increased associated measurement errors (see below).

Within the resolution of the data, the displacement

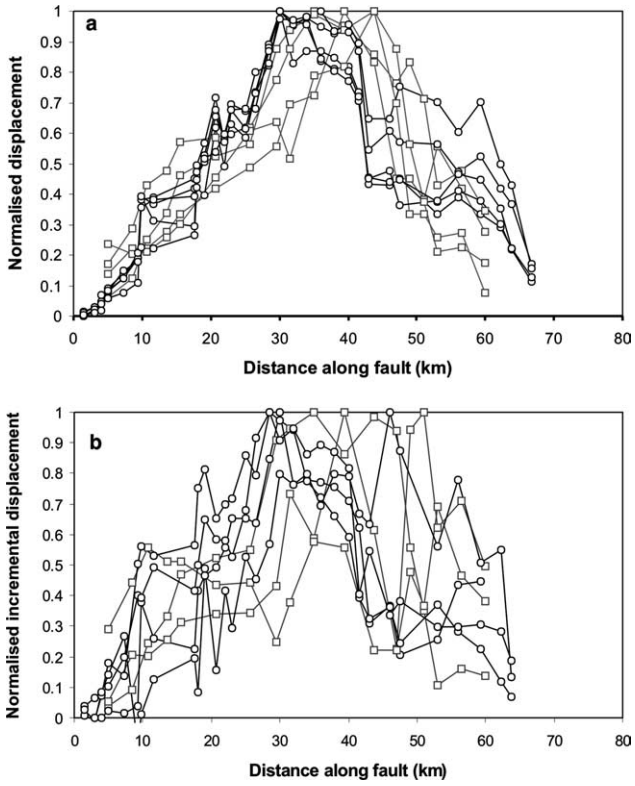

Fig. 10. Normalised along-strike displacement profiles for the Cape Egmont Fault. The profiles enable the displacement pattern on each horizon to be compared directly and indicate that the shape of the profiles has not changed significantly through time. (a) Profiles normalised to the maximum displacement for each of the nine dated horizons using data in Fig. 9. (b) Profiles normalised to the maximum displacement that accrued during the increments of time between the dated horizons. Incremental displacements were determined by calculating the difference in displacement between adjacent horizons (e.g. displacement of 3.7 Ma horizon minus displacement of 3.2 Ma horizon). Black lines and open circles show horizons 1.6–3.7 Ma in age, while grey lines and open squares display horizons 14–225 ka in age.

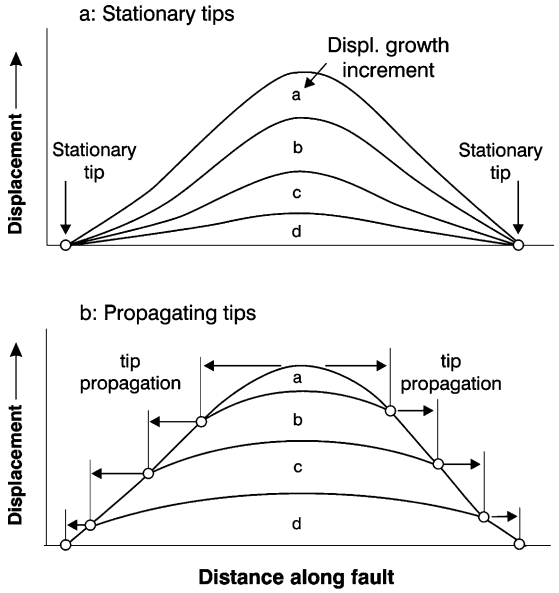

Fig. 11. Schematic diagram showing the distinction between along-strike displacement profiles which show no lateral propagation (a) and those that indicate lateral propagation (b). In both diagrams the areas labelled a–d represent progressively younger increments of displacement. For diagram (b) the fault nucleates at its centre and propagates at constant rates from this point. Refer to text for further discussion of this figure.

profiles in Fig. 9 converge towards common points approximately coincident with current fault-tip positions. Fault tips are more difficult to locate using Late Quaternary displacement profiles, particularly to the north, because of difficulties in resolving small displacements. Nevertheless the location at the southern tip of the fault appears to have been stable in the Late Quaternary and is approximately coincident with the long-term position of the tip, determined from the deep multi-channel seismic data. Although the position of the northern tip of the Late Quaternary fault trace is less clear, the profiles for all horizons, except the seabed, converge at a distance of 65–70 km along the fault (Fig. 9b). The seabed fault scarp becomes sub-resolution at a distance of about 60 km along the fault and therefore represents a minimum fault length at the seafloor.

In a syn-faulting growth sequence, displacement profiles for progressively younger horizons that converge towards a common tip location indicate little or no fault propagation (Fig. 11a), a feature that is consistent with the constant fault-length model (Walsh et al., 2002). Conversely, for propagating faults the intersection point of progressively younger horizons would be expected to migrate away from the maximum displacement (Fig. 11b; Childs et al., 1995, 2003). The profile geometries in Fig. 9 are consistent with the generic model presented schematically in Fig. 11a, supporting the conclusion that the tips of the CEF remained approximately fixed with no fault propagation and constant fault length since 3.2 Ma. This is not an isolated occurrence and normal faults with stationary tip positions and no propagation have been reported in other extensional basins (Childs et al., 1995, 2003; Morewood and Roberts, 1999; Poulimenos, 2000; Meyer et al., 2002). For the CEF the maximum trace length in the Pliocene/Recent formed in <0.5 Ma during which time 55% of the total displacement accrued on the fault.

The reactivated nature of the CEF provides a physical basis for the initial period of rapid lengthening of the fault between 3.7 and 3.2 Ma. The cross-section presented in Fig. 4 is typical of data along the length of the fault, suggesting that the earliest recorded displacement on the structure occurred during the Late Cretaceous, with subsequent inversion and reactivation during the Late Miocene. At the commencement of the latest period of normal displacement the fault was probably no more than 500 m below the seabed and the post-Miocene faulting appears to have reactivated the pre-existing structure along its entire length. We therefore favour a model in which the currently active fault occupies a zone of pre-existing crustal heterogeneity, which has been observed or inferred for

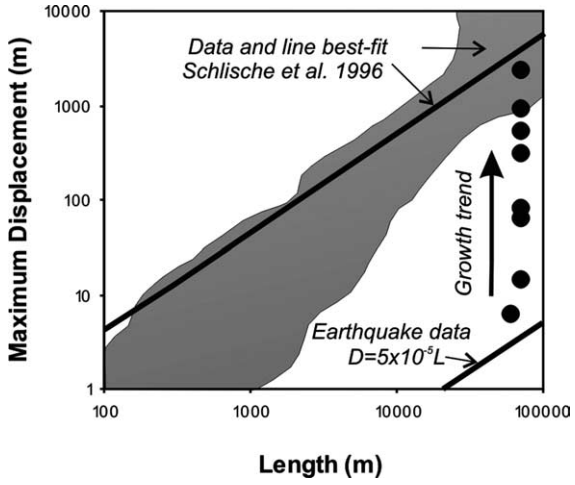

Fig. 12. Log–log plot of maximum displacement vs. fault length for each of the mapped horizons. Data are inferred to represent an upward growth sequence (for further discussion see text and Walsh et al. (2002)). Shaded area outlines the field of existing empirical data (Schlische et al., 1996), while the average position of earthquake data is from Wells and Coppersmith (1994).

many fault systems, and within post-Miocene strata grew mainly by up-dip propagation to establish its final length. For such a model, up-dip propagation rates of as low as 1 km/Ma would be required to establish the entire length of the CEF in 0.5 Ma. This value is at the lower end of lateral propagation rates of <23 km/Ma reported in the literature (e.g. Morewood and Roberts, 2002 and references therein; Childs et al., 2003), and is significantly lower than the 70 km/Ma lateral propagation rate required to form the present length of the CEF without upward propagation.

As the fault length (L) remained approximately fixed from deposition of the 3.2 Ma horizon to the present, and because the total displacement (D) progressively increased during the life of the fault, the ratio of D to L increases from 10^{-4} to 3×10^{-2} with increasing horizon age (Fig. 12). These data cover the range of expected ratios between single earthquake ruptures (e.g. Wells and Coppersmith, 1994) and inactive faults (e.g. Walsh and Watterson, 1988; Cowie and Scholz, 1992b; Gillespie et al., 1992; Schlische et al., 1996). The progressive change in D and L relations in Fig. 13 can be considered a growth trend for that period of time over which fault length remained near constant. Similar vertical growth trends on D vs. L plots are proposed by Walsh et al. (2002) in a new fault growth model and are consistent with observations from normal faults in the Aegean (Morewood and Roberts, 1999; Poulimenos, 2000) and Timor Sea (Meyer et al., 2002). Near-constant fault lengths over millions of years are also consistent with faults that appear to show little or no increase in fault length between successive earthquakes (e.g. Lindvall et al., 1989).

Late Quaternary displacements on the main fault decrease adjacent to active synthetic splays that intersect the main fault (Nodder, 1993, 1994). These displacement lows are partly removed by aggregating displacement on the

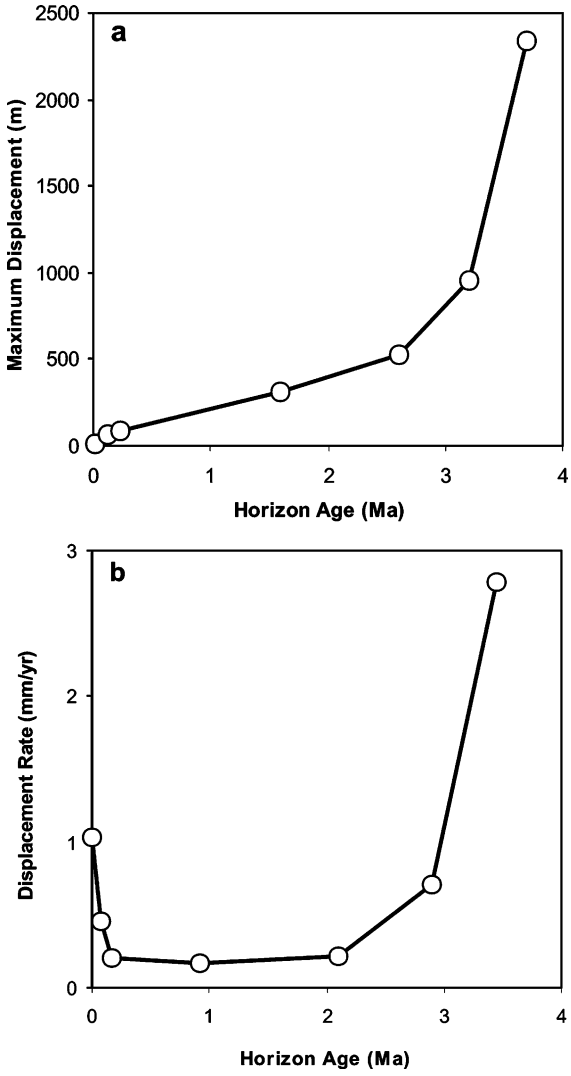

Fig. 13. Plots showing the evolution of maximum displacement (a) and maximum displacement rates (b) in the last 4 Ma. See text for explanation of the derivation of the data.

splays with those on the main fault. Slight deficits that remain may be accounted for by sub-resolution ductile deformation between the splays and the main fault. The aggregated displacement profiles for Late Quaternary horizons and the seabed are more irregular than the long-term profiles, particularly northeast of the maxima (compare Fig. 9a and b) where displacement is accommodated on an array of splays. To explain this greater irregularity one could invoke earthquake-slip models in which zones of displacement deficit over the Late Quaternary were regions of surplus displacement prior to this time interval (e.g. Contreras et al., 2000; Gupta and Scholz, 2000). We do not, however, subscribe to this explanation, because there is no clear antipathetic relationship between earlier and later displacement profiles and because there are, as yet, no independent grounds for suggesting that displacement deficits of some tens of metres can be sustained on time scales greater than 0.1 Ma. Instead we suggest that

irregularities in the Late Quaternary profiles arise from conversion of fault displacements to ductile strains, with bed rotation and gentle folding between synthetic splays within the relatively unconsolidated Late Quaternary sediments, and from limitations in resolution and increased measurement error (e.g. Pliocene–Pleistocene horizons $\leq \pm 15$–35% as opposed to $\leq \pm 50\%$ for the seabed scarp).

4. Temporal changes in displacement rates

Displacement rates on normal faults within some extensional basins have been shown to be approximately constant over periods of a million years or greater (Nicol et al., 1997). Approximately constant displacement rates can be envisaged where faults reach their final length early in the evolution of the system and regional strain rates are constant. In circumstances where faults continue to grow in length throughout their life and/or where some faults die (Roberts et al., 2002), displacement rates on individual faults may vary over millions of years. How often changes in displacement rate mainly reflect variations in the magnitudes of regional strain rate and how often they arise from local evolution of a fault or fault array is uncertain.

Incremental displacement rates can be determined if up-dip throw gradients were approximately zero during each increment of fault growth. In these circumstances accumulation of throw over the period of time between deposition of two sedimentary horizons is equal to the difference in displacement on these horizons (Childs et al., 1993, 2003; Clausen et al., 1994). Displacements on the CEF (Fig. 13a) are used in conjunction with horizon ages to calculate incremental displacement rates (Fig. 13b). We use maximum displacements on each horizon to calculate rates. It would also be valid to use average displacements, although our results and general conclusions are not influenced by which of these measures are used. Based on our assessment of the uncertainties associated with the measurement of horizon displacements and ages, we suggest that uncertainties on the incremental displacement rates may be as much as about $\pm 50\%$. Displacement rates varied significantly through time, with high values of ca. 0.7–2.8 mm/yr and ca. 0.4–1.1 mm/yr during 3.7–2.6 Ma and in the last ca. 100 ka, respectively, separated by about 2.5 Ma when the rates were ca. 0.1–0.2 mm/yr and generally low. These variations range up to about an order of magnitude and, as they cannot be entirely accounted for by uncertainties in the data, offer insights into the faulting process.

High displacement rates observed on the CEF during the Late Quaternary could, in part, reflect temporal clustering of earthquakes, which has been observed over time-scales of tens to hundreds of thousands of years (e.g. Wallace, 1987; Coppersmith, 1989; Sieh et al., 1989; Grant and Sieh, 1994; Marco et al., 1996). It seems unlikely, however, that the dramatic adjustment in displacement rate between 2 and 3 Ma ago could be attributed to short-term changes in earthquake clustering. Instead, these long-term changes in fault behaviour could be due to: (i) transfer of displacement from the CEF to other faults within the Taranaki Graben, as suggested by Roberts et al. (2002) for Central Italy, or (ii) graben-wide temporal fluctuations in strain rates. Unequivocally discriminating between these models requires displacement data for all faults within Taranaki Graben over the last 3.7 Ma and such data are not currently available. Strain rates on the Hikurangi subduction margin, 200 km to the east (Fig. 2) may, however, provide a basis for the variable displacement rates on the CEF. Both shortening along the subduction margin and back arc extension in Taranaki Graben are driven by subduction of the Pacific Plate beneath the overriding Australian Plate (e.g. Walcott, 1978). Analysis of reverse faults and folds along the Hikurangi margin for the last 10 Ma indicates three time intervals of relatively rapid shortening punctuated by periods of slower shortening at 1–2.5 and 3.7–5 Ma (Melhuish, 1990; Nicol et al., 1996, 2002; Beanland et al., 1998). Temporal variations in rates of shortening along the subduction margin and extension on the CEF are therefore similar, from which we infer that the broad pattern of changes in Fig. 13b principally reflects plate-boundary-wide fluctuations in strain rates and not local migration of activity between faults within the graben. As the relative plate motion vector between the plates has remained approximately constant over the last ca. 6 Ma (DeMets et al., 1994; Walcott, 1998), we suggest that periods of elevated strain rates in the overriding plate result from an increase in the degree to which the plates are locked, as would be expected to arise from increased subduction of sediments or from the onset of subduction of the Hikurangi Plateau (e.g. Davy, 1993; Beaumont et al., 1999).

5. Long-term earthquake-slip behaviour

The manner in which maximum magnitude and recurrence interval of earthquakes on an individual fault evolves over millions of years is intimately linked to the growth of the fault surface during this time. If the dimensions of a fault surface increase throughout its life (e.g. Watterson, 1986; Walsh and Watterson, 1988; Cowie and Scholz, 1992b; Schlische et al., 1996), then following the well established empirical relation between coseismic slip and fault rupture length (e.g. Scholz, 1982; Wells and Coppersmith, 1994), the maximum magnitude and slip for an earthquake that ruptures the entire fault surface must also increase. In these circumstances, the recurrence interval would have to decrease if, for example, constant displacement rates were to be maintained (e.g. Cowie and Scholz, 1992a; Walsh and Watterson, 1992). Estimates can be made of the maximum earthquake magnitude and average recurrence interval on a fault at any point in time, if the rates of displacement and tip-line propagation are constrained. While displacement

rates of many active faults are known for the Late Quaternary, information on fault propagation rates is uncommon, and opportunities to characterise average earthquake behaviour over periods of >100 ka are extremely rare.

The displacement profiles in Figs. 9a and 10 suggest that the fault reached its maximum length during the first 0.5 Ma of growth after which time fault length remained approximately constant. Therefore, the maximum magnitudes and slip for earthquakes that ruptured the entire trace length at the seabed must also have been relatively constant. Using the empirical magnitude–rupture length relations from Wells and Coppersmith (1994), maximum earthquake magnitudes for the fault would range from ca. 7.1 to 7.2 for each increment of fault growth, which are similar to those estimated by Nodder (1994). Events of this magnitude and rupture length (i.e. ca. 70 km) are, on average, associated with maximum displacements at the surface of ca. 3.5 m (using the ratio of slip to rupture length of 5×10^{-5} from Wells and Coppersmith (1994)); with about two and four events of this size required to produce the observed seabed scarp and 14 ka displacement profile, respectively.

In order to estimate the minimum number of earthquakes that would be necessary to produce the reported along-strike displacements, we compare the observed profiles for all horizons in the growth sequence with models constructed by linearly scaling displacements of the 14 ka horizon (Fig. 14). For the model, displacements on the 14 ka horizon were either divided (seabed scarp) or multiplied (pre-14 ka horizons) by an integer value (here referred to as the scaling factor) in order to minimise the difference in mean arithmetic displacement between the model and observed profiles. The 14 ka horizon was used to construct the models, as opposed to the seabed scarp, because this horizon has lower errors on displacement values and because the scarp may have been subject to modification by seabed processes. Displacement profiles of the seabed scarp and 14 ka horizon are, however, comparable in shape (Fig. 14a) and the following conclusions are not significantly influenced by which of these two surfaces was chosen to model. Given the extent to which this approach magnifies displacement anomalies on the 14 ka horizon it was expected that the model results would locally depart from the observed profiles. In general terms, however, the position of the maximum displacement and the fault tips for the last few earthquakes, as represented by the 14 ka horizon, are comparable with all other time increments. These data are consistent with the maximum rupture length and slip distribution for large earthquakes on the fault being approximately constant suggesting that of the six models in Fig. 1 the CEF is best represented by diagrams (a) or (b). In the absence of slip data for individual earthquakes throughout the growth of the fault we cannot, however, discriminate between the characteristic-slip (Fig. 1a) and variable-slip (Fig. 1b) earthquake models.

Given the changes in fault strike and the number of splays intersecting the main slip surface of the CEF (Fig. 3) and the irregularities in the displacement profiles (Fig. 9), it remains possible that the fault was segmented and did not rupture in its entirety during each large magnitude earthquake (Nodder, 1994). While the difference between segmented and unsegmented earthquake models would be significant for earthquake hazard assessment, it has less impact on our analysis of slip accumulation. This is because stress can be transferred from a given ruptured segment to an adjacent segment resulting in sequential rupture of all segments over periods of hundreds of years or less (e.g. Stein et al., 1997). For such a model the period of time between earthquakes on adjacent segments is short by comparison with the time between earthquakes on each segment. Therefore, the number of earthquakes estimated using our approach can be thought of as the number of the largest sized earthquakes, or the number of earthquake cycles (where each segment ruptures once per cycle) required to produce the observed slip. The number of notional earthquakes required to produce the optimal match between the scaled displacement on the 14 ka horizon and the remaining seven profiles is simply the product of the scaling factor and four (i.e. the number events with 3.5 m maximum slip required to produce the maximum displacement on the 14 ka surface). The number of earthquakes ranges from 2 to 344 for the seabed scarp and 3.2 Ma horizon, respectively (Figs. 14a–f and 15a). If, however, the active fault occupied the pre-existing fault dimensions instantaneously on a geological timescale, and the length remained constant for the entire duration of deformation, then 722 large magnitude earthquakes would be required over the post-Miocene life (3.7 Ma) of the fault (Fig. 14g). This large number of earthquakes is, however, a factor of 2–10 lower than the number of slip events predicted for increasing fault-length growth models constructed using the present length and maximum displacement of the CEF (e.g. Watterson, 1986; Walsh and Watterson, 1988; Cowie and Scholz, 1992a). These models apply to faults that propagated laterally, and radially, throughout growth, with earthquake size increasing with fault length, and the extent to which they differ from our estimated number of earthquakes is a direct reflection of the rapid creation of the final length of the CEF.

Perhaps of greater interest though is the temporal variability in the number of large magnitude earthquakes for each period of time, which can be expressed as a mean recurrence interval (Fig. 15b). Mean earthquake recurrence intervals in Fig. 15b were calculated by dividing the minimum number of earthquakes for each increment of time (Fig. 14) by its duration. Mean recurrence intervals vary through time from ca. 1.3 to 18 ka and are, as would be expected, diametrically opposed to fluctuations in displacement rate. For example, displacement rates of ca. 2.8 (3.7–3.2 Ma) and 0.2 mm/yr (2.6–1.6 Ma) were associated with average recurrence intervals of ca. 1.3 and 18 ka, respectively. This relation is a direct reflection of the fixed fault

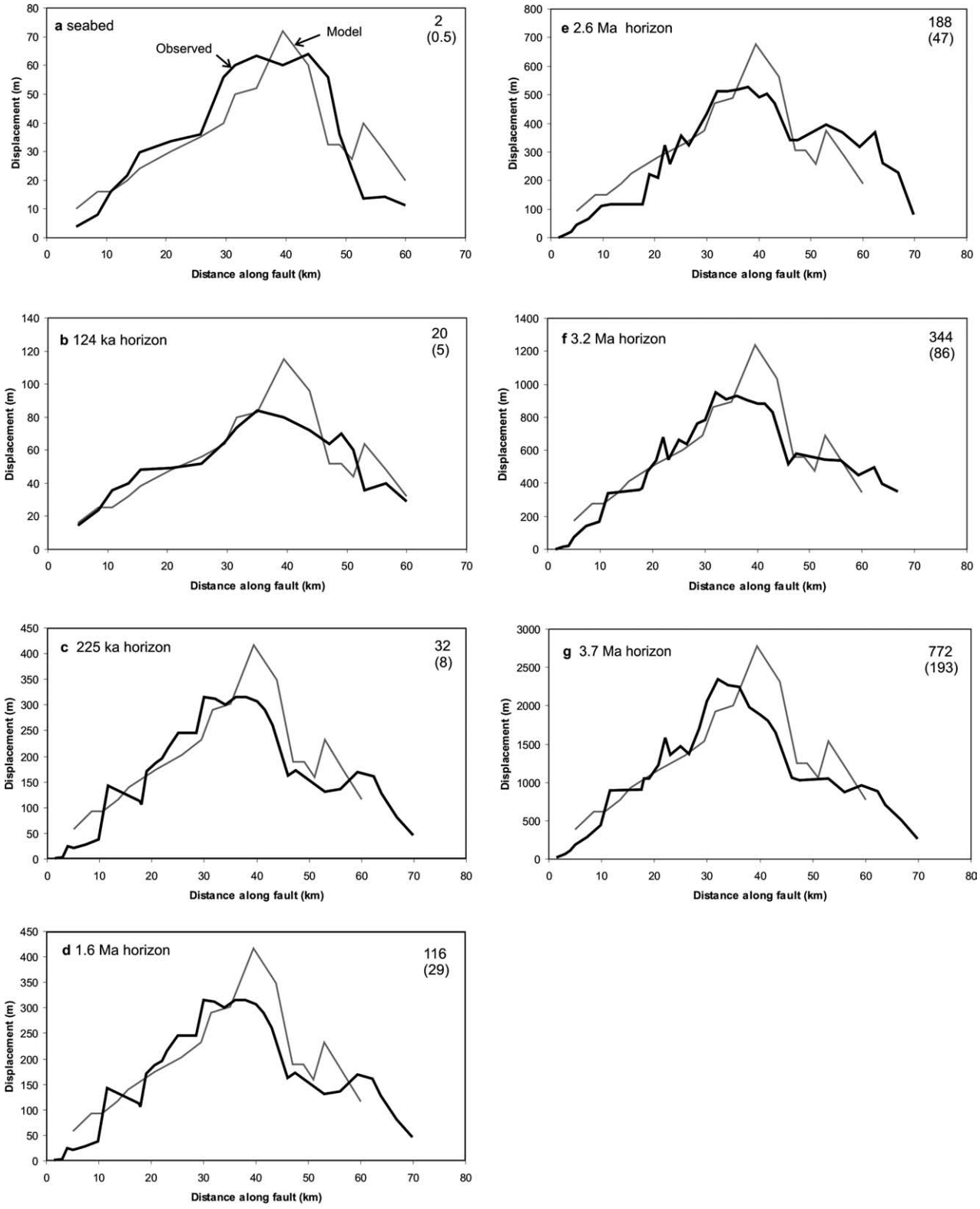

Fig. 14. Modelled and observed displacement profiles constructed for the (a) seabed scarp, (b) 124 ka horizon, (c) 225 ka horizon, (d) 1.6 Ma horizon, (e) 2.6 Ma horizon, (f) 3.2 Ma horizon and (g) 3.7 Ma horizon. Models constructed by linear scaling of the 14 ka displacement profile. The minimum number of earthquakes required to produce the model profiles is indicated in the right-hand corner of each graph. The number in brackets, below the minimum number of earthquakes, is the scaling factor and indicates the integer value by which displacements on the 14 ka profile have been multiplied to produce the model profile. For further discussion of the model profiles and explanation of the minimum number of earthquakes refer to the text.

length and proportional earthquake maximum slip to rupture length scaling, a feature which demands that increases in displacement rates must result in a proportional decrease in recurrence interval. As changes in displacement rates on the CEF are driven by adjustments in regional strain rates, mean recurrence intervals of earthquakes on the CEF will also broadly reflect changes in regional strain rates (Nicol et al., 2004). This conclusion is consistent with the suggestion that, to a first order, changes in regional strain rates are accommodated mainly by adjustments in fault displacement rates and not by a change in the number of active faults (Clausen et al., 1994; Nicol et al., 1997).

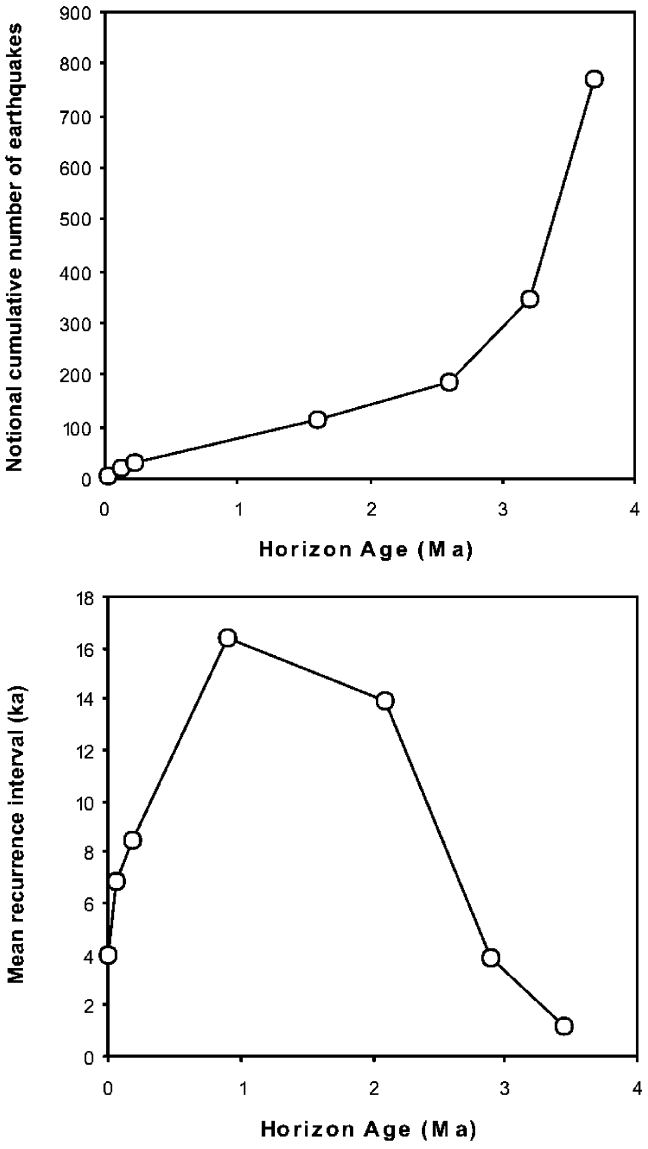

Fig. 15. Plots showing the evolution of the minimum number of earthquakes (a) and the mean recurrence intervals (b) for each increment of time between the formation of dated horizons. Refer to text for derivation of plots.

6. Conclusions

The CEF is active and commenced its most recent phase of displacement about 3.7 Ma ago. Strike-parallel displacement profiles for seven syn-faulting horizons and the seabed indicate that the location of the fault tips and maximum displacement remained approximately stationary for at least 3.2 Ma during which time about half of the total displacement accrued on the fault. Near-constant fault lengths in post-Miocene strata were inherited from a pre-existing fault and formed rapidly, primarily in response to up-dip propagation of the fault surface. Consequently, as earthquake-rupture length scales with magnitude and slip, the maximum earthquake slip and magnitude on the fault also remained constant for at least 3.2 Ma. This stability contrasts with displacement rates on the fault, which varied by an order of magnitude (ca. 0.18–2.8 mm/yr), and were associated with diametrically opposed and proportional changes in earthquake recurrence intervals (ca. 1.3–18 ka). Modifications to the displacement rates and recurrence intervals resulted mainly from graben-wide changes in rates of extension.

Acknowledgements

This paper is the result of studies completed with financial support from the Royal Society of New Zealand Marsden Fund (GNS 902) and EU 4th Framework Grant (JOF3-CT97-0036). We thank members of the Fault Analysis Group, in particular Conrad Childs and Tom Manzocchi, for discussions on fault-related growth issues. Jon Bull, Dave Sanderson and Richard Norris are thanked for their constructive reviews of the manuscript. Institute of Geological and Nuclear Sciences contribution number 3130.

References

Barnett, J.A.M., Mortimer, J., Rippon, J.H., Walsh, J.J., Watterson, J., 1987. Displacement geometry in the volume containing a single normal fault. American Association of Petroleum Geologists Bulletin 71, 925–937.

Beanland, S., Melhuish, A., Nicol, A., Ravens, J., 1998. Structure and deformation history of the inner forearc region, Hikurangi Subduction Margin, New Zealand. New Zealand Journal of Geology and Geophysics 41, 325–342.

Beaumont, C., Ellis, S., Pfiffner, A., 1999. Dynamics of sediment subduction–accretion at convergent margins: short-term modes, long-term deformation, and tectonic implications. Journal of Geophysical Research 104, 17573–17601.

Berryman, K.R., Beanland, S., 1991. Variation in fault behaviour in different tectonic provinces of New Zealand. Journal of Structural Geology 13, 177–189.

Bonilla, M.G., Mark, R.K., Lienkaemper, J.J., 1984. Statistical relations among earthquake magnitude, surface rupture length, and surface fault displacement. Bulletin of the Seismological Society of America 74, 2379–2411.

Cartwright, J.A., Trudgill, B., Mansfield, C.S., 1995. Fault growth by

segment linkage: an explanation for scatter in maximum displacement and trace length data from the Canyonlands Grabens of S.E. Utah. Journal of Structural Geology 17, 1319–1326.

Childs, C., Easton, S.J., Vendeville, B.C., Jackson, M.P.A., Lin, S.T., Walsh, J.J., Watterson, J., 1993. Kinematic analysis of faults in a physical model of growth faulting above a viscous salt analogue. Tectonophysics 228, 313–329.

Childs, C., Watterson, J., Walsh, J.J., 1995. Fault overlap zones within developing normal fault systems. Journal of the Geological Society of London 152, 535–549.

Childs, C., Nicol, A., Walsh, J.J., Watterson, J., 2003. The growth and propagation of synsedimentary faults. Journal of Structural Geology 25, 633–648.

Clausen, O.-R., Korstgard, J.A., Petersen, K., McCann, T., O'Reilly, B.M., Shannon, P.M., Howard, C.B., Mason, P.J., Walsh, J.J., Watterson, J., 1994. Systematics of faults and fault arrays, in: Helbig, K. (Ed.), Modeling the Earth for Oil Exploration. Final Report of the CEC's Geoscience Program 1990–1993. Elsevier, pp. 205–316.

Contreras, J., Anders, M.H., Scholz, C.H., 2000. Growth of a normal fault system: observations from the Lake Malawi basin of the east African rift. Journal of Structural Geology 22, 159–168.

Coppersmith, K.J., 1989. On spatial and temporal clustering of paleoseismic events. Seismological Research Letters 59, 299–304.

Cowie, P.A., Scholz, C.H., 1992a. Growth of faults by accumulation of seismic slip. Journal of Geophysical Research 97, 11085–11095.

Cowie, P.A., Scholz, C.H., 1992b. Displacement–length scaling relationships for faults: data synthesis and discussion. Journal of Structural Geology 14, 1149–1156.

Davy, B., 1993. The influence of subducting plate buoyancy on subduction of the Hikurangi–Chatham Plateau beneath the North Island, New Zealand, in: Watkins, J., Zhigiang, F., McMillen, K. (Eds.), Advances in the Geology and Geophysics of Continental Margins American Association of Petroleum Geologists Memoir, 53, pp. 75–91.

Dawers, N.H., Anders, M.H., Scholz, C.H., 1993. Growth of normal faults: displacement–length scaling. Geology 21, 1107–1110.

DeMets, C., Gordon, R.G., Argus, D.F., Stein, S., 1994. Effect of recent revisions to the geomagnetic reversal time scale on estimates of current plate motions. Geophysical Research Letters 21, 2191–2194.

Elliott, D., 1976. The energy balance and deformation mechanisms of thrust sheets. Philosophical Transactions of the Royal Society of London A 283, 289–312.

Gilbert, G.K., 1884. A theory of earthquakes of the Great Basin, with practical application (from the Salt Lake Tribune of September 30, 1883). American Journal of Science, 3rd Series 27, 49–53.

Gillespie, P.A., Walsh, J.J., Watterson, J., 1992. Limitations of dimension and displacement data from single faults and the consequences for data analysis and interpretation. Journal of Structural Geology 14, 1157–1172.

Grant, L.B., Sieh, K., 1994. Paleoseismic evidence for clustered earthquakes on the San Andreas fault in the Carrizo Plain, California. Journal of Geophysical Research 99, 6819–6841.

Gupta, A., Scholz, C.H., 2000. A model of normal fault interaction based on observations and theory. Journal of Structural Geology 22, 865–879.

King, P.R., Thrasher, G.P., 1992. Post-Eocene development of the Taranaki Basin, New Zealand: convergent overprint of a passive margin, in: Watkins, J.F., Zhigiang, F., McMillen, K. (Eds.), Advances in the Geology and Geophysics of Continental Margins American Association of Petroleum Geologists Memoir, 53, pp. 93–118.

King, P.R., Thrasher, G.P., 1996. Cretaceous and Cenozoic Geology and Petroleum Systems of the Taranaki Basin, New Zealand, Institute of Geological & Nuclear Sciences Monograph 13, Lower Hutt, New Zealand 1996.

van der Linden, W.J.M., 1971. High resolution bathymetry, an aid to geophysical prospecting. Geophysics 36, 960–962.

Lindvall, S., Rockwell, T., Hudnut, K., 1989. Evidence for prehistoric earthquakes on the Superstition Hills fault from offset geomorphic features. Bulletin of the Seismological Society of America 79, 342–361.

McCalpin, J.P., Forman, S.L., Lowe, M., 1994. Re-evaluation of Holocene faulting at the Kaysville trench site, Wasatch fault zone, Utah. Tectonics 13, 1–16.

Machette, M.N., Personius, S.F., Nelson, A.R., 1992. The Wasatch fault zone, U.S.A.. Annales Tectonicae, Special Issue Supplement to Volume VI, 5–39.

McLeod, A.E., Dawers, N.H., Underhill, J.R., 2000. The propagation and linkage of normal faults: insights from the Strathspey–Brent–Statfjord fault array, northern North Sea. Basin Research 12, 263–284.

Mandl, G., 1987. Discontinuous fault zones. Journal of Structural Geology 9, 105–110.

Marco, S., Stein, M., Agnon, A., 1996. Long-term earthquake clustering: a 50,000-year paleoseismic record in the Dead Sea Graben. Journal of Geophysical Research 101, 6179–6191.

Marrett, R., Almendinger, R.W., 1991. Estimates of strain due to brittle faulting: sampling of fault populations. Journal of Structural Geology 13, 735–738.

Melhuish, A., 1990. Late Cenozoic deformation along the Pacific–Australian plate margin, Dannevirke region, New Zealand. Unpublished M.Sc. thesis, Victoria University of Wellington, New Zealand.

Meyer, V., Nicol, A., Childs, C., Walsh, J.J., Watterson, J., 2002. Progressive localisation of strain during the evolution of a normal fault system in the Timor Sea. Journal of Structural Geology 24, 1215–1231.

Morewood, N.C., Roberts, G.P., 1999. Lateral propagation of the surface trace of the South Alkyonides normal fault segment, central Greece: its impact on models of fault growth and displacement–length relationships. Journal of Structural Geology 21, 635–652.

Morewood, N.C., Roberts, G.P., 2002. Surface observations of active normal fault propagation: implications for growth. Journal of the Geological Society of London 159, 263–272.

Morley, C.K., Vanhauwaert, P., De Batist, M., 2000. Evidence for high frequency cyclic fault activity from high resolution seismic reflection survey, Rukwa Rift, Tanzania. Journal of the Geological Society of London 157, 983–994.

Muraoka, H., Kamata, H., 1983. Displacement distribution along minor fault traces. Journal of Structural Geology 5, 483–495.

Nicol, A., Melhuish, A., Beanland, S., 1996. Episodic deformation of the Hikurangi Forearc during the last 8 Ma. Geological Society of New Zealand Miscellaneous Publication 91A, 137.

Nicol, A., Walsh, J.J., Watterson, J., Underhill, J.R., 1997. Displacement rates of normal faults. Nature 390, 157–159.

Nicol, A., Van Dissen, R., Vella, P., Alloway, B., Melhuish, A., 2002. Growth of contractional structures during the last 10 Ma, Hikurangi forearc, New Zealand. New Zealand Journal of Geology and Geophysics 45, 365–385.

Nicol, A., Walsh, J., Manzocchi, T., Morewood, N. 2004. Displacement rates and average recurrence intervals on normal faults. Journal of Structural Geology, in press.

Nodder, S.D., 1993. Neotectonics of the offshore Cape Egmont Fault Zone, Taranaki Basin. New Zealand Journal of Geology and Geophysics 36, 167–184.

Nodder, S.D., 1994. Characterizing potential offshore seismic sources using high-resolution geophysical and seafloor sampling programs: an example from Cape Egmont fault zone, Taranaki shelf, New Zealand. Tectonics 13, 641–658.

Peacock, D.C.P., Sanderson, D.J., 1991. Displacements, segment linkage and relay ramps in normal fault zones. Journal of Structural Geology 13, 721–733.

Petersen, K., Clausen, O.-R., Korstgård, J.A., 1992. Evolution of a salt-related listric growth fault near the D-1 well, block 5605, Danish North Sea: displacement history and salt kinematics. Journal of Structural Geology 14, 565–577.

Poulimenos, G., 2000. Scaling properties of normal fault populations in the western Corinth Graben, Greece: implications for fault growth in large strain settings. Journal of Structural Geology 22, 307–322.

Reyners, M., 1989. New seismicity 1964–87: an interpretation. New Zealand Journal of Geology and Geophysics 32, 307–315.

Roberts, G., Michetti, A.M., Cowie, P., Morewood, N.C., Papanikolaou, I., 2002. Fault slip-rate variations during crustal-scale strain localisation, central Italy. Geophysical Research Letters 29, doi: 10.1029/2001L013529.

Robinson, R., Calhaem, I.M., Thomson, A.A., 1976. The Opunake, New Zealand, earthquake of 5 November 1974. New Zealand Journal of Geology and Geophysics 19, 335–345.

Schlische, R.W., Young, S.S., Ackermann, R.V., Gupta, A., 1996. Geometry and scaling relations of a population of very small rift-related normal faults. Geology 24, 683–686.

Scholz, C.H., 1982. Scaling laws for large earthquakes: consequences for physical models. Bulletin of the Seismological Society of America 72, 1–14.

Scholz, C.H., 1990. The Mechanics of Earthquakes and Faulting. Cambridge University Press, New York.

Schwartz, D.P., Coppersmith, K.J., 1984. Fault behavior and characteristic earthquakes: examples from the Wasatch and San Andreas fault zones. Journal of Geophysical Research 89, 5681–5698.

Shell BP Todd Oil Services Ltd, 1970. Well resume Maui-2, Taranaki offshore concession no. 682a. Unpublished open-file Petroleum report 541. Ministry of Commerce, New Zealand.

Shell BP Todd Oil Services Ltd, 1970. Well resume Maui-4, Taranaki offshore concession no. 682a. Unpublished open-file Petroleum report 543. Ministry of Commerce, New Zealand.

Shell BP Todd Oil Services Ltd, 1977. Well resume Tane-1. Petroleum prospecting licence no. 38007, sub area A. Unpublished open-file Petroleum report 698. Ministry of Commerce, New Zealand.

Shell BP Todd Oil Services Ltd, 1982. Well resume Kiwa-1. Petroleum prospecting licence no. 38055, Taranaki offshore. Unpublished open-file Petroleum report 880. Ministry of Commerce, New Zealand.

Sieh, K.E., Stuiver, M., Brillinger, D., 1989. A more precise chronology of earthquakes produced by the San Andreas fault in southern California. Journal of Geophysical Research 94, 603–623.

Stein, R.S., King, G.C., Rundle, J.B., 1988. The growth of geological structures by repeated earthquakes. 2. Field examples of continental dip-slip faults. Journal of Geophysical Research 93, 13,319–13,331.

Stein, R., Barka, A., Dieterich, J., 1997. Progressive failure on the North Anatolian Fault since 1939 by earthquake stress triggering. Geophysical Journal International 128, 594–604.

Thrasher, G.P., 1990. Tectonics of the Taranaki Rift. New Zealand Oil Exploration Conference Proceedings. Petroleum and Geothermal Unit, Energy and Resources Division, Ministry of Commerce, New Zealand, pp. 124–133.

Thrasher, G.P., 1991. Neogene activity on the Cape Egmont Fault Zone, Taranaki Basin. Geological Society of New Zealand Miscellaneous Publication 59A, 138.

Thrasher, G.P., King, P.R., Cook, R.A., 1995. Taranaki Basin Petroleum atlas. 50 maps plus booklet. Institute of Geological & Nuclear Sciences Ltd, Lower Hutt.

Treagus, S.H., Lisle, R.J., 1997. Do principal surfaces of stress and strain always exist? Journal of Structural Geology 19, 997–1010.

Trudgill, B., Cartwright, J., 1994. Relay ramp forms and normal fault linkages; Canyonlands National Park, Utah. Bulletin of the Geological Society of America 106, 1143–1157.

Walcott, R.I., 1978. Present tectonics and late Cenozoic evolution of New Zealand. Geophysical Journal of the Royal Astronomical Society 52, 137–164.

Walcott, R.I., 1998. Modes of oblique compression: late Cenozoic tectonics of the South Island of New Zealand. Reviews in Geophysics 36, 1–26.

Wallace, R.E., 1987. Grouping and migration of surface faulting and variations in slip rates on faults in the Great Basin Province. Bulletin of the Seismological Society of America 77, 868–876.

Walsh, J.J., Watterson, J., 1987. Distributions of cumulative displacement and seismic slip on a single normal fault surface. Journal of Structural Geology 9, 1039–1046.

Walsh, J.J., Watterson, J., 1988. Analysis of the relationship between the displacements and dimensions of faults. Journal of Structural Geology 10, 239–247.

Walsh, J.J., Watterson, J., 1991. Geometric and kinematic coherence and scale effects in normal fault systems, in: Roberts, A.M., Yielding, G., Freeman, B. (Eds.), The Geometry of Normal Faults Geological Society of London Special Publication, 56, pp. 193–203.

Walsh, J.J., Watterson, J., 1992. Populations of faults and fault displacements and their effects on estimates of fault-related regional extension. Journal of Structural Geology 14, 701–712.

Walsh, J.J., Nicol, A., Childs, C., 2002. An alternative model for the growth of faults. Journal of Structural Geology 24, 1669–1675.

Walsh, J.J., Bailey, W.R., Childs, C., Nicol, A., Bonson, C.G., 2003. Formation of segmented normal faults: a 3-D perspective. Journal of Structural Geology 25, 1251–1262.

Watterson, J., 1986. Fault dimensions, displacements and growth. Pure and Applied Geophysics 124, 365–373.

Wells, D.L., Coppersmith, K.J., 1994. New empirical relationships among magnitude, rupture length, rupture width, rupture area, and surface displacement. Bulletin of the Seismological Society of America 84, 974–1002.

Wesnousky, S.G., 1994. The Gutenberg–Richter distribution or characteristic earthquake distribution: which is it? Bulletin of the Seismological Society of America 84, 1940–1959.

Yeats, R.S., Sieh, K., Allen, C.R., 1997. The Geology of Earthquakes. Oxford University Press, New York.